Title: **Physics-informed Guided Wavefield Data Completion**

Authors : Harsha Vardhan Tetali
Joel B. Harley

ABSTRACT

Ultrasonic wavefields are widely employed in nondestructive testing and structural health monitoring to detect and evaluate structural damage. However, measuring wavefields continuously throughout space poses challenges and can be costly. To address this, we propose a novel approach that combines the wave equation with computer vision algorithms to visualize wavefields. Our algorithm incorporates the wave equation, which encapsulates our knowledge of wave propagation, to infer the wavefields in regions where direct measurement is not feasible. Specifically, we focus on reconstructing wavefields from partial measurements, where the wavefield data from large continuous regions are missing. The algorithm is tested on experimental data demonstrating its effectiveness in reconstructing the wavefields at unmeasured regions. This also benefits in reducing the need for expensive equipment and enhancing the accuracy of structural health monitoring at a lower cost. The results highlight the potential of our approach to advance ultrasonic wavefield imaging capabilities and open new avenues for Nondestructive testing and structural health monitoring.

INTRODUCTION

Structural Health Monitoring (SHM) employs nondestructive methods, notably ultrasonic guided waves, to assess structural integrity [1–3]. Guided waves' ability to cover vast areas with minimal intensity loss allows their use in various structures, such as pipelines [2, 4–9], bridges [10, 11], concrete structures [12], steel cables [13–15], and components of aircraft [16–21]. These waves, detected by high-resolution systems like scanning laser Doppler vibrometers [22], provide information about structure composition and defects. Full wavefield acquisition may not always be feasible; thus, reconstruction algorithms are often employed initially. The pursuit of efficient wavefield data handling and interpretation techniques has become a significant research area.

Some popular wavefield imaging reconstruction techniques are:

- **Back-Propagation** [23]: This is a common method used in ultrasound imaging

Harsha Vardhan Tetali, email: vardhanh71@gmail.com. SmartData Lab, Department of Electrical and Computer Engineering, University of Florida, Gainesville, FL, USA.

and involves the inversion of data collected from multiple sensors to produce an image.

- **Seismic Migration** [24]: This method involves the extrapolation of wavefield data to a desired image plane and is commonly used in seismology and geophysics.
- **Compressed Sensing** [25]: This is a recent method that exploits the sparsity of wavefield data in a transformed domain to reconstruct images with fewer measurements than traditional methods.
- **Time Reversal** [26]: This is a process of reversing the time evolution of a wavefield to focus the energy onto a target location and is used in medical imaging and nondestructive testing.

Traditional wavefield analysis techniques are algorithmically limited and often struggle with complex data, especially when significant data chunks are missing or when reflections from boundaries occur. The incorporation of physics-informed machine learning, specifically Physics-Informed Neural Networks (PINNs) [27], shows promise in addressing these issues, enhancing our capacity to solve and identify partial differential equations (PDEs) [28–31]. However, the complexity of these "black-box" neural network models can hinder interpretability and guaranteed convergence, besides requiring extensive training data, computational resources, and training time.

We propose a balanced solution - a wave-informed decomposition technique to learn approximate wavefield modes. This method reconstructs wavefields by enforcing their compliance with the wave equation. We demonstrate that our algorithm can reconstruct wavefields in large unmeasurable regions, using information from surrounding regions, effectively performing data imputation or completion.

WAVE-PHYSICS INFORMED DECOMPOSITION

The Wave-physics Informed Decomposition (WID) provides a fresh approach to wavefield data decomposition, breaking down input wavefields into constituent wave modes, each with a unique propagation velocity obtained through the WID algorithm. This algorithm ensures each mode follows a discrete wave equation, adhering to the fundamental physical principles of wave propagation. The inherent resistance to discontinuity in wave modes aids in recovering large missing data segments in wavefields.

WID represents an advancement in physics-informed machine learning, offering a simpler yet powerful alternative to deep learning. By integrating fundamental physics principles, WID creates a more intuitive, interpretable model capable of handling complex wavefield data, aligning with the trend towards more interpretable, robust, and physically consistent AI models.

Tensorial Representation of Discrete Wavefields

Let's imagine a wavefield, denoted as $f(x, y, t)$, that is continuous and exists on a finite structure within a finite time frame. For ease of understanding, assume that x has the range defined by $[0, L_x]$, y is defined in $[0, L_y]$, and t in $[0, T]$.

Now, let's sample this wavefield at N_x, N_y, and N_t points in the respective dimensions of space (x and y) and time (t). The intervals between these sample points in space and time are represented as $\Delta x = L_x/N_x$, $\Delta y = L_y/N_y$, and $\Delta t = T/N_t$, signifying the sampling periods for each dimension.

Subsequently, we form a tensor, $\mathbf{U} \in N_x \times N_y \times N_t$. This tensor, in essence, captures the sampled values of our original wavefield $f(x, y, t)$ across the defined spatial and temporal dimensions.

$$\mathbf{U}_{i_x,i_y,i_t} = f\left(i_x\Delta x, i_y\Delta y, i_t\Delta t\right). \tag{1}$$

The tensor $\mathbf{U}$ stands as a discretized representation of the wavefield $f(x, y, t)$. In the decomposition algorithm we outline, we deal with vectorized forms of the tensors, which are symbolized as vec($\mathbf{U}$).

The Wave Equation Discretized

The wave equation for a wave traveling in two spatial dimensions at a speed denoted by c can be expressed as follows:

$$\frac{\partial^2 u(x,y,t)}{\partial x^2} + \frac{\partial^2 u(x,y,t)}{\partial y^2} = \frac{1}{c^2}\frac{\partial^2 u(x,y,t)}{\partial t^2} \tag{2}$$

Presuming that $\mathbf{U}$ is the tensor representing the discretized form of the wavefield $u(x, y, t)$, the corresponding discrete form of the wave equation can be described as follows:

$$\begin{aligned}\left(\boldsymbol{I}_t \otimes \boldsymbol{I}_y \otimes \boldsymbol{L}_x + \boldsymbol{I}_t \otimes \boldsymbol{L}_y \otimes \boldsymbol{I}_x\right) \text{vec}(\mathbf{U}) \\ = \frac{1}{c^2}\left(\boldsymbol{L}_t \otimes \boldsymbol{I}_y \otimes \boldsymbol{I}_x\right) \text{vec}(\mathbf{U})\end{aligned} \tag{3}$$

where $\boldsymbol{I}_t$,$\boldsymbol{I}_y$,$\boldsymbol{I}_x$ are identity matrices with sizes of N_t, N_x, and N_y, respectively. In addition, $\boldsymbol{L}_x$, $\boldsymbol{L}_y$, and $\boldsymbol{L}_y$ are Laplacian operators, discrete approximations of the second derivation operation, for their respective dimensions. Finally, $\otimes$ represents the Kronecker production operation and vec represents the vectorization operation.

The Objective Function for Modal Extraction

Considering the discretized wave data, represented by the tensor $\mathbf{Y} \in \mathbb{R}^{N_x \times N_y \times N_t}$, our objective is to decompose this tensor $\mathbf{Y}$ into an aggregate of multiple tensors. Each of these tensors should conform to a discrete variant of the wave equation. The principle underlying this decomposition process can be aptly articulated as follows:

$$\mathbf{Y} = \mathbf{U}_1 + \mathbf{U}_2 + \cdots + \mathbf{U}_m \tag{4}$$

in this context, each $\mathbf{U}_i$ (where i belongs to the set $[m]$) is required to fulfill the conditions of a discretized form of the wave equation.

To take advantage of linear algebra principles and cast the problem in the context of matrix factorization, it proves beneficial to vectorize (or flatten) the tensors and operate within the framework of vectors. To cater to this matrix factorization structure, we

rephrase equation 4 in a vectorized form as follows:

$$\boldsymbol{y} = \sum_{i=1}^{m} \boldsymbol{u}_i \tag{5}$$

where $\boldsymbol{y} = \text{vec}(\mathbf{Y})$ and $\boldsymbol{u}_i = \text{vec}(\mathbf{U}_i)$, for $i \in [m]$. Assume that each $\boldsymbol{u}_i$ can be represented as $\boldsymbol{D}_i x_i$, where x_i acts as a scaling factor and $\boldsymbol{D}_i$ is a column of matrix $\boldsymbol{D}$. We can then reformulate our representation as $\boldsymbol{y} = \boldsymbol{D}\boldsymbol{x}$. In this equation, $\boldsymbol{x}$ comprises elements x_i (for i in the set $[m]$). This formulation embodies the matrix factorization aspect of our objective function.

In the initial framework, prior to vectorization, $\mathbf{U}_i$ was required to adhere to a discrete form of the wave equation. This necessitates a similar stipulation on $\boldsymbol{D}_i$ (considering x_i are scalars), albeit in a slightly altered format. Let's denote the discrete version of the wave equation, incorporating the wave velocity parameter c_i, as $\mathcal{W}c_i(\boldsymbol{D}_i) = 0$. To impose the structural characteristics derived from the wave equation, we aim to minimize $\min_{c_i} \|\mathcal{W}c_i(\boldsymbol{D}_i)\|_2^2$, incorporating it as a component of the regularizer.

Moreover, we strive to limit the number of velocity modes to a minimum. We accomplish this by adding the squared Frobenius norms of both $\boldsymbol{D}$ and $\boldsymbol{x}$. It is well known that this strategy tends to induce low-rank solutions in the product $\boldsymbol{D}\boldsymbol{x}$ due to its link with the variational form of the nuclear norm, as suggested in the works of [32], [33], [34], [35].

As a result, we derive the regularizer as

$$\Theta(\boldsymbol{D}, \boldsymbol{x}) = \sum_{i=1}^{M} \bar{\theta}(\boldsymbol{D}_i, x_i) \tag{6}$$

where $\gamma > 0$ is a tunable parameter and $\bar{\theta}(\boldsymbol{D}_i, x_i) = \gamma \min_{c_i} \|\mathcal{W}_{c_i}(\boldsymbol{D}_i)\| + \|\boldsymbol{D}_i\|_2^2 + x_i^2$. The ultimate problem we aim to solve, framed in the form of an optimization objective, is as follows:

$$\begin{aligned} \min_{M} \min_{\boldsymbol{D},\boldsymbol{x},\boldsymbol{c}} \; & \frac{1}{2}\|\boldsymbol{y} - \boldsymbol{D}\boldsymbol{x}\|_2^2 \\ & + \frac{\lambda}{2}\left(\sum_{i=1}^{M} \gamma \min_{c_i > 0} \|\mathcal{W}_{c_i}(\boldsymbol{D}_i)\|_2^2 + \|\boldsymbol{D}_i\|_2^2 + x_i^2\right). \end{aligned} \tag{7}$$

The linear operator $\mathcal{W}_{c_i}(.)$ is contingent on the value of c_i. Consequently, it's possible to define a matrix in such a way that, $\mathcal{W}_{c_i}(\boldsymbol{v}) = \boldsymbol{A}_{c_i}\boldsymbol{v}$. For,

$$\boldsymbol{A}_c = \boldsymbol{L}_x \otimes \boldsymbol{I}_y \otimes \boldsymbol{I}_t + \boldsymbol{I}_x \otimes \boldsymbol{L}_y \otimes \boldsymbol{I}_t - \frac{1}{c^2}\boldsymbol{I}_x \otimes \boldsymbol{I}_y \otimes \boldsymbol{L}_t \tag{8}$$

and $\lambda > 0$ is the regularization weighting the term $\Theta(\boldsymbol{D}, \boldsymbol{x})$.

THE OPTIMIZATION ALGORITHM

Using a flowchart as a guide (refer to Fig. 1), we outline the algorithm employed to solve this optimization problem, with theoretical details available in [34–36]. The

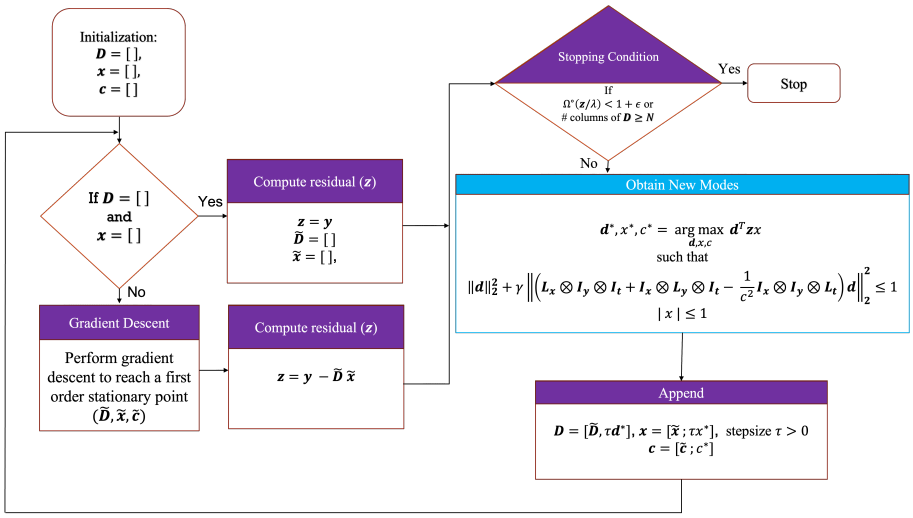

Figure 1. Wave-physics informed decomposition flowchart

algorithm begins with an empty matrix $\boldsymbol{D}$ and an empty vector $\boldsymbol{x}$, incrementing the number of columns in $\boldsymbol{D}$ by 1 and correspondingly adjusting the size of vector $\boldsymbol{x}$ in each iteration (refer to the "Obtain New Modes" block in Fig 1, highlighted in blue, which generates the column to be appended).

The algorithm ceases operation in proximity to global optimality due to the stopping condition $\Omega^\circ(\boldsymbol{z}/\lambda) < 1 + \epsilon$ (see equation 9), which guarantees that the acquired $\boldsymbol{D}$ and $\boldsymbol{x}$ are within $\mathcal{O}(\epsilon)$ of the optimal solution ([35], Prop. 4), given a user-defined $\epsilon > 0$. We additionally also specify a practical stopping condition where the algorithm stops after a specified N size for the number of columns in $\boldsymbol{D}$.

$$\Omega_\theta^\circ\left(\frac{\boldsymbol{z}}{\lambda}\right) = \max_{\boldsymbol{d},x,c_i} \boldsymbol{d}^\top \left(\frac{\boldsymbol{z}}{\lambda}\right) x$$
$$\text{s.t. } \|\boldsymbol{d}\|_2^2 + \gamma \|\boldsymbol{A}_c \boldsymbol{d}\|_2^2 \leq 1, |x| \leq 1. \tag{9}$$

Note that the above optimization problem is often called the polar problem and it is used in obtaining new modes and also in the stopping condition. λ is the regularization constant as defined in the previous section and $\boldsymbol{z}$ is usually the error between the aggregate of the decompositions so far and the actual data. $\boldsymbol{A}_c$ is as defined in equation 8.

RESULTS AND DISCUSSION

The algorithm is run on ultrasonic wavefield data obtained by exciting an aluminum plate with a chirp signal ranging from 0 to 300kHz. The measured data then has a peak frequency at 130.6kHz. Fig. 2 shows the snapshots of the data considered at different time points. We observe the wavefield originating from a single location. In addition, there is a secondary source / point scatterer (i.e., damage). We also observe that the wave reflects from the boundaries at the edges of the spatial area.

We test our algorithm on this dataset by blinding a centered continuous region (Fig. 3(a)). We demonstrate the effectiveness of our method in reconstructing the wavefields at the unmeasured regions (Fig. 3 (a) and (b)) and show its capability to reconstruct the

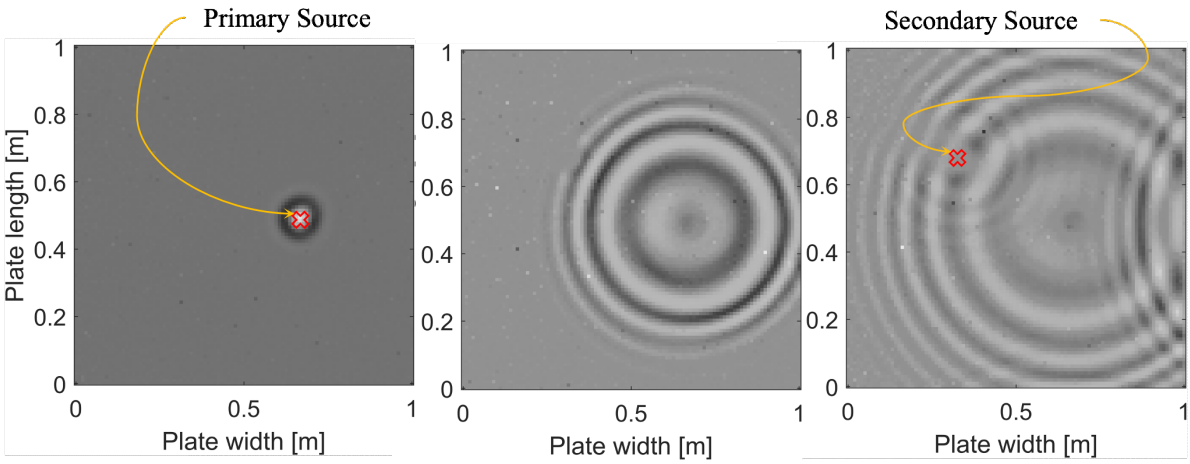

Figure 2. Snapshots of data at different time frames

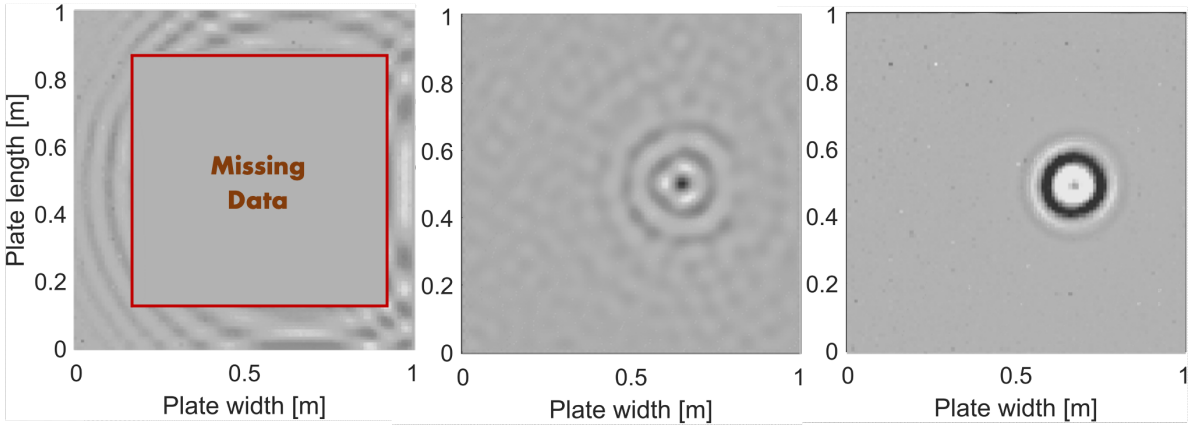

Figure 3. (a) The partial wavefield at a time stamp (the data in the red box is assumed to be unmeasurable). (b) The reconstructed wavefield (at a different timestamp) clearly indicating the location of the source. (c) The actual wavefield at almost the same timestamp as in (b) confirming the location of the source.

exact location of the source, even when the source is in the unmeasurable region. Fig. 3 (c) shows the true wavefield and location of the source. This approach enhances the capabilities of ultrasonic wavefield imaging and opens new avenues for Nondestructive testing and structural health monitoring.

CONCLUSIONS

This paper introduces the wave-physics informed decomposition algorithm, a novel technique for reconstructing large missing data sections in structural health monitoring. Our findings validate its successful application in regions where direct measurements are unattainable. Future studies will evaluate its performance in detecting primary and secondary sources, thereby consolidating its application in nondestructive testing and structural health monitoring. This algorithm marks a stride in wavefield reconstruction and promises to enhance ultrasonic wavefield imaging and structural health monitoring.

ACKNOWLEDGMENTS

This work is partially supported by NSF EECS-1839704 and NSF CISE-1747783.

REFERENCES

1. Cawley, P. 2003. "Practical long range guided wave inspection – managing complexity," in *Proc. of the Review of Progress in Quantitative Nondestructive Evaluation*, vol. 22, pp. 22–40.
2. Cawley, P. 2007. "Practical guided wave inspection and applications to structural health monitoring," in *Proc. of the Australasian Congress on Applied Mechanics*, Brisbane, p. 10.
3. Cawley, P. 2018. "Structural health monitoring: Closing the gap between research and industrial deployment," *Structural Health Monitoring*, 17(5):1225–1244.
4. Davies, J. and P. Cawley. 2009. "The application of synthetic focusing for imaging crack-like defects in pipelines using guided waves," *IEEE Trans. Ultrason. Ferroelectr. Freq. Control*, 56(4):759–771.
5. Liu, C., J. Harley, N. O'Donoughue, Y. Ying, M. H. Altschul, M. Bergés, J. H. Garrett, D. W. Greve, J. M. F. Moura, I. J. Oppenheim, and L. Soibelman. 2012. "Robust change detection in highly dynamic guided wave signals with singular value decomposition," in *2012 IEEE International Ultrasonics Symposium*, IEEE, Dresden, pp. 483–486.
6. Ying, Y., L. Soibelman, J. Harley, N. O'Donoughue, J. H. Garrett, Y. Jin, J. M. F. Moura, and I. J. Oppenheim. 2010. "A data mining framework for pipeline monitoring using time reversal," in *Proc. of SIAM Conference on Data Mining*, SIAM, Columbus, Ohio.
7. Ying, Y., J. H. Garrett, Jr., J. Harley, I. J. Oppenheim, J. Shi, and L. Soibelman. 2013. "Damage Detection in Pipes under Changing Environmental Conditions Using Embedded Piezoelectric Transducers and Pattern Recognition Techniques," *J. Pipeline Syst. Eng. Pract.*, 4(1):17–23.
8. Rizzo, P., I. Bartoli, A. Marzani, and F. L. di Scalea. 2005. "Defect Classification in Pipes by Neural Networks Using Multiple Guided Ultrasonic Wave Features Extracted After Wavelet Processing," *J. Pressure Vessel Technol.*, 127(3):294–303.
9. Li, J. and J. Rose. 2002. "Angular-Profile Tuning of Guided Waves in Hollow Cylinders Using a Circumferential Phased Array," *IEEE Trans. Ultrason. Ferroelectr. Freq. Control*, 49(12):1720–1729.
10. Chen, S., F. Cerda, J. Guo, J. B. Harley, Q. Shi, P. Rizzo, J. Bielak, J. H. Garrett, and J. Kovacević. 2013. "Multiresolution classification with semi-supervised learning for indirect bridge structural health monitoring," in *2013 IEEE International Conference on Acoustics, Speech and Signal Processing*, IEEE, Vancouver, BC, pp. 3412–3416.
11. Holford, K. M., A. W. Davies, R. Pullin, and D. C. Carter. 2001. "Damage Location in Steel Bridges by Acoustic Emission," *J. Intell. Mater. Syst. Struct.*, 12(8):567–576.
12. Chong, K. P., N. J. Carino, and G. Washer. 2003. "Health monitoring of civil infrastructures," *Smart Mater. Struct.*, 12(3):483–493.
13. Baltazar, A., C. D. Hernandez-Salazar, and B. Manzanares-Martinez. 2010. "Study of wave propagation in a multiwire cable to determine structural damage," *NDT and E Int.*, 43(8):726–732.
14. Rizzo, P. 2004. "Wave Propagation in Multi-Wire Strands by Wavelet-Based Laser Ultrasound," *Exp. Mech.*, 44(4):407–415.
15. Rizzo, P. and F. Lanza di Scalea. 2001. "Acoustic emission monitoring of carbon-fiber-reinforced-polymer bridge stay cables in large-scale testing," *Exp. Mech.*, 41(3):282–290.

16. Ihn, J.-B. and F.-K. Chang. 2008. "Pitch-catch Active Sensing Methods in Structural Health Monitoring for Aircraft Structures," *Structural Health Monitoring*, 7(1):5–19.
17. Worden, K., G. Manson, and D. Allman. 2003. "Experimental Validation of a Structural Health Monitoring Methodology: Part I. Novelty Detection on a Laboratory Structure," *J. Sound Vib.*, 259(2):323–343.
18. Leckey, C. A. C., M. D. Rogge, and F. Raymond Parker. 2014. "Guided waves in anisotropic and quasi-isotropic aerospace composites: three-dimensional simulation and experiment," *Ultrasonics*, 54(1):385–394.
19. Staszewski, W. J., S. Mahzan, and R. Traynor. 2009. "Health monitoring of aerospace composite structures – Active and passive approach," *Compos. Sci. Technol.*, 69(11-12):1678–1685.
20. Qiu, L., S. Yuan, X. Zhang, and Y. Wang. 2011. "A time reversal focusing based impact imaging method and its evaluation on complex composite structures," *Smart Mater. Struct.*, 20(10):105014.
21. Salamone, S., I. Bartoli, F. Lanza Di Scalea, and S. Coccia. 2009. "Guided-wave Health Monitoring of Aircraft Composite Panels under Changing Temperature," *J. Intell. Mater. Syst. Struct.*, 20(9):1079–1090.
22. Castellini, P., M. Martarelli, and E. Tomasini. 2006. "Laser Doppler Vibrometry: Development of advanced solutions answering to technology's needs," *Mechanical Systems and Signal Processing*, 20(6):1265–1285, ISSN 0888-3270, special Issue: Laser Doppler Vibrometry.
23. Natterer, F. and F. Wubbeling. 1995. "A propagation-backpropagation method for ultrasound tomography," *Inverse Problems*, 11(6):1225, doi:10.1088/0266-5611/11/6/007.
24. Kim, S., Y. S. Kim, and W. Chung. 2022. "Efficient least-squares reverse time migration using local cross-correlation imaging condition," *Journal of Geophysics and Engineering*, 19(3):376–388, ISSN 1742-2132, doi:10.1093/jge/gxac027.
25. Keshmiri Esfandabadi, Y., L. De Marchi, N. Testoni, A. Marzani, and G. Masetti. 2018. "Full Wavefield Analysis and Damage Imaging Through Compressive Sensing in Lamb Wave Inspections," *IEEE Transactions on Ultrasonics, Ferroelectrics, and Frequency Control*, 65(2):269–280, doi:10.1109/TUFFC.2017.2780901.
26. Esmersoy, C. and M. L. Oristaglio. 1988. "Reverse-time wave-field extrapolation, imaging, and inversion," *Geophysics*, 53(7):920–931.
27. Raissi, M., P. Perdikaris, and G. Karniadakis. 2019. "Physics-informed neural networks: A deep learning framework for solving forward and inverse problems involving nonlinear partial differential equations," *Journal of Computational Physics*, 378:686–707, ISSN 0021-9991.
28. Shukla, K., P. C. Di Leoni, J. Blackshire, D. Sparkman, and G. E. Karniadakis. 2020. "Physics-informed neural network for ultrasound nondestructive quantification of surface breaking cracks," *Journal of Nondestructive Evaluation*, 39:1–20.
29. Yu, Y., C. Wang, X. Gu, and J. Li. 2019. "A novel deep learning-based method for damage identification of smart building structures," *Structural Health Monitoring*, 18(1):143–163.
30. Moseley, B., A. Markham, and T. Nissen-Meyer. 2020. "Solving the wave equation with physics-informed deep learning," *arXiv preprint arXiv:2006.11894*.
31. Rasht-Behesht, M., C. Huber, K. Shukla, and G. E. Karniadakis. 2022. "Physics-Informed Neural Networks (PINNs) for Wave Propagation and Full Waveform Inversions," *Journal of Geophysical Research: Solid Earth*, 127(5):e2021JB023120.
32. Srebro, N. and A. Shraibman. 2005. "Rank, trace-norm and max-norm," in *Proc. of the International Conference on Computational Learning Theory*, Springer, pp. 545–560.
33. Recht, B., M. Fazel, and P. A. Parrilo. 2010. "Guaranteed minimum-rank solutions of linear

matrix equations via nuclear norm minimization," *SIAM review*, 52(3):471–501.

34. Haeffele, B., E. Young, and R. Vidal. 2014. "Structured low-rank matrix factorization: Optimality, algorithm, and applications to image processing," in *Proc. of the International Conference on Machine Learning*, pp. 2007–2015.
35. Haeffele, B. D. and R. Vidal. 2019. "Structured low-rank matrix factorization: Global optimality, algorithms, and applications," *IEEE Transactions on Pattern Analysis and Machine Intelligence*, 42(6).
36. Tetali, H. V., J. B. Harley, and B. D. Haeffele. 2021. "Wave-Informed Matrix Factorization with Global Optimality Guarantees," *arXiv preprint arXiv:2107.09144*.